NANO LETTERS

pubs.acs.org/NanoLett Letter

Competing Charge Transfer and Screening Effects in Two-Dimensional Ferroelectric Capacitors

Jiawei Huang,[#] Changming Ke,[#] Zhuang Qian, and Shi Liu*

Cite This: https://doi.org/10.1021/acs.nanolett.4c01362 Read Online

ACCESS | Metrics & More | Article Recommendations | Supporting Information

ABSTRACT: Two-dimensional (2D) ferroelectrics promise ultrathin flexible nanoelectronics, typically utilizing a metal−ferroelectric−metal sandwich structure. Electrodes can either contribute free carriers to screen the depolarization field, enhancing nanoscale ferroelectricity, or induce charge doping, disrupting the long-range crystalline order. We explore electrodes' dual roles in 2D ferroelectric capacitors, supported by first-principles calculations covering a range of electrode work functions. Our results reveal volcano-type relationships between ferroelectric−electrode binding affinity and work function, which are further unified by a quadratic scaling between the binding energy and the transferred interfacial charge. At the monolayer limit, charge transfer dictates the ferroelectric stability and switching properties. This general characteristic is confirmed in various 2D ferroelectrics including α-In_2Se_3, $CuInP_2S_6$, and SnTe. As the ferroelectric layer's thickness increases, the capacitor stability evolves from a charge-transfer-dominated state to a screening-dominated state. The delicate interplay between these two effects has important implications for 2D ferroelectric capacitor applications.

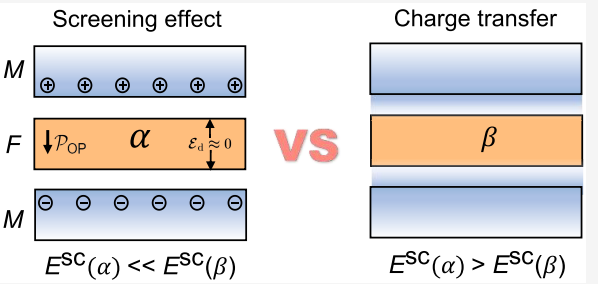

KEYWORDS: *ferroelectric capacitor; two-dimensional ferroelectric materials; screening effect; charge transfer*

The discovery of 2D ferroelectrics, specifically those with out-of-plane polarization ($\mathcal{P}_{OP}$) such as α-In_2Se_3[1,2] and $CuInP_2S_6$,[3,4] has profoundly reshaped our understanding of ferroelectricity at the nanoscale. Recent experiments show that van der Waals (vdW) stacked bilayers, even if they are composed of nonferroelectric monolayers, can be transformed into ferroelectrics through sliding and twisting operations,[5−9] thereby greatly expanding the family of 2D ferroelectrics with $\mathcal{P}_{OP}$. These 2D ferroelectrics, benefiting from the uniform atomic thickness, absence of surface dangling bonds, and scalability in the lateral dimension, are intensely studied as critical components in a wide array of device types, including those used in neuromorphic computing and ultrathin flexible nanoelectronics.[10,11] Notably, 2D α-In_2Se_3 stands out for its exceptional carrier mobility, semiconducting bandgap, and robust room-temperature monolayer-limit $\mathcal{P}_{OP}$ even against unscreened depolarization field ($\mathcal{E}_d$) under open-circuit (OC) electrical boundary conditions.[1,12] Shortly after its discovery in 2017, this 2D ferroelectric was swiftly adopted in the fabrication of ferroelectric semiconductor field effect transistors[12] and ferroelectric memristors.[13]

Most ferroelectric-based electronics, such as ferroelectric random-access memory and ferroelectric tunneling junction,[14,15] employ a two-terminal metal−ferroelectric−metal (MFM) sandwich structure in which a ferroelectric is sandwiched between two metal electrodes. It is widely recognized that the interface between metal and ferroelectric layers can have significant impacts on device properties.[16−19] Specifically, the screening of interfacial polarization bound charges by the metallic electrodes is crucial for the stabilization of $\mathcal{P}_{OP}$ normal to the interface. It can be reasonably deduced that $\mathcal{P}_{OP}$ in a 2D ferroelectric, intrinsically stable under OC boundary conditions, would be further stabilized when placed between electrodes as the screening could reduce the depolarization field. However, another perspective arises when considering the work functions of the electrodes. The 2D ferroelectric in an MFM might experience charge doping due to the charge transfer between the electrodes and the ferroelectric layer.[17,20−22] Given the ultrathin nature of 2D ferroelectrics and the sensitivity of spontaneous polarization to charge doping, a pressing question emerges: Which effect predominates at the nanoscale, and consequently, how does this influence the stability of $\mathcal{P}_{OP}$ considering these two competing effects? Using In_2Se_3 as a representative example, here, we elaborate the potential outcomes stemming from the interplay between screening and interfacial charge transfer. As shown in Figure 1a, monolayer In_2Se_3 consists of five atomic

Received: March 21, 2024
Revised: May 16, 2024
Accepted: May 16, 2024

https://doi.org/10.1021/acs.nanolett.4c01362
Nano Lett. XXXX, XXX, XXX−XXX

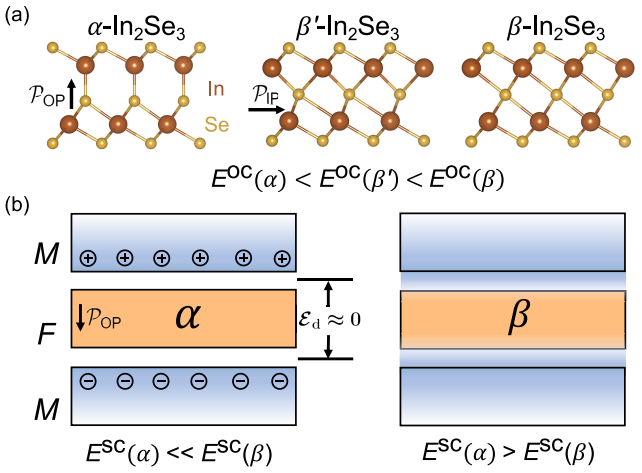

Figure 1. (a) Structures of 2D α-In_2Se_3 with out-of-plane polarization ($\mathcal{P}_{OP}$), β'-In_2Se_3 with in-plane polarization ($\mathcal{P}_{IP}$), and nonpolar β-In_2Se_3. An isolated free-standing monolayer is under open-circuit (OC) electrical boundary conditions. (b) Illustration of the potential outcomes of an MFM capacitor resulting from the competition between screening and interfacial charge transfer effects. The screening of the depolarization field by the electrodes could further stabilize the α phase under short-circuit (SC) boundary conditions (left). In contrast, electrodes with low work functions might effectively charge dope the α phase to suppress the ferroelectricity (right).

planes of triangular lattices in a Se−In−Se−In−Se order and can crystallize in multiple phases. In monolayer α-In_2Se_3 (space group $P3m1$), a vertical displacement of the middle Se layer along the z-axis leads to $\mathcal{P}_{OP}$; in contrast, the β' phase exhibits an in-plane polarization ($\mathcal{P}_{IP}$) due to an in-plane shift of the central Se layer. The high-temperature β phase is nonpolar with a space group of $P\bar{3}m1$. Previous studies based on first-principles density functional theory (DFT) calculations have revealed that the free-standing monolayer β-In_2Se_3 and β'-In_2Se_3 are higher in energy (E) by 0.15 and 0.05 eV per 5-atom unit cell (uc), respectively, than the α phase under OC conditions, that is, $E^{OC}(\alpha) < E^{OC}(\beta') < E^{OC}(\beta)$.[1,23] This is consistent with a relatively high ferroelectric−paraelectric ($\alpha \rightarrow \beta$) phase transition temperature of 700 K as observed in 3 nm thick α-In_2Se_3 crystals.[2] In an MFM heterostructure incorporating a monolayer α-In_2Se_3, a potential outcome is that the α phase may be further stabilized relative to the β phase under short-circuit (SC) boundary conditions. This stabilization could occur because the free carriers in the capping electrodes might screen the surface polarization bound charges, thereby reducing the depolarization field. Such a scenario, where the screening effect is predominant, is denoted as $E^{SC}(\alpha) \ll E^{SC}(\beta)$ in Figure 1b. Conversely, electrodes with low work functions might effectively dope the monolayer α-In_2Se_3 with electrons. This could lead to a strong screening of the dipole−dipole interactions, which are crucial for the emergence of ferroelectricity. Such charge doping likely causes $E^{SC}(\alpha) > E^{SC}(\beta)$, potentially quenching the ferroelectricity. Considering these conflicting outcomes, comprehending the intricate interplay between screening and interfacial charge transfer becomes essential for advancing and fine-tuning nanoelectronics based on 2D ferroelectrics.

Here, we address the fundamental question above by analyzing the binding energy (E_b) between monolayer In_2Se_3 in different phases and a range of metal electrodes with varying work functions (W_M), employing first-principles DFT calculations. Our results reveal a volcano-type relationship with a flattened top between E_b and W_M. A unified relationship between E_b and the amount of charge (Q) transferred at the interface is established, given by $E_b = -\gamma Q^2$ with γ as a constant independent of the polar state or phase. In particular, the nonpolar β phase binds more strongly to low-work-function (LW) electrodes compared to the polar α and β' phases. Consequently, monolayer In_2Se_3 favors the nonpolar β phase when sandwiched by LW electrodes, whereas it transitions to the polar α phase in the presence of high-work-function (HW) electrodes. The substantial impact of interfacial charge transfer on the ferroelectric stability proves to be a prevalent feature for 2D ferroelectrics including $CuInP_2S_6$ (CIPS) and SnTe.[24] Finally, we observe a crossover from charge-transfer dominance to screening dominance with increasing thickness of the ferroelectric layer in an MFM structure composed of symmetric LW electrodes and In_2Se_3. This transition is accompanied by the spontaneous formation of a buffer layer near one electrode, yielding an intrinsically asymmetric MFM capacitor. These insights into the mechanisms governing charge transfer and screening at the nanoscale have important implications for the design of 2D ferroelectric-based ultrathin nanoelectronics.

All DFT calculations are performed using Vienna *ab initio* simulation package (VASP)[25,26] with the Perdew−Burke−Ernzerhof (PBE) density functional[27] and the projector augmented wave (PAW) method.[28] Various factors, including the interface chemistry and strain conditions due to the electrode−ferroelectric lattice mismatch, can substantially affect the electronic structure of the metal−ferroelectric interface, making it challenging to disentangle their individual contributions. Here, we select 2D metallic materials with lattice constants close to the ground-state values of α-In_2Se_3 as electrodes. This approach offers two key advantages. First, the electrode−ferroelectric interface in vdW heterostructures of 2D materials is free from dangling bonds and less affected by the lattice mismatch. Second, the extensive variety of 2D metallic materials available in DFT-based database, such as C2DB,[29,30] allows for the selection of electrodes with both the desired lattice constants and a range of work functions. We therefore examine 18 2D electrodes with work functions ranging from 2 to 10 eV (details in the Supporting Information). When screening the 2D material database to select 2D metal electrodes of different work functions, we used the criterion that the lattice mismatch between the electrode and α-In_2Se_3 should be below 2%. Therefore, fixing the in-plane lattice constants of different electrodes to the ground-state value of the monolayer of α-In_2Se_3 (4.06 Å) during structural optimizations introduces a relatively small strain effect. The work functions of 2D electrodes are calculated based on the optimized structures with the in-plane lattice fixed at 4.06 Å. The van der Waals correction is considered using the Grimme's DFT-D3 method during the structural optimization of MFM capacitors. All calculations are performed using a plane-wave cutoff energy of 500 eV, a 7 × 7 × 1 Monkhorst−Pack k-point grid, an energy convergence threshold of 1×10^{-8} eV, and a force convergence threshold of 1×10^{-7} eV/Å. The vacuum layer along the z direction is thicker than 15 Å, and the dipole correction is employed to remove the artificial electric field and unphysical dipole−dipole interactions between different periodic images.

https://doi.org/10.1021/acs.nanolett.4c01362
Nano Lett. XXXX, XXX, XXX−XXX

We start by computing the binding energy of 2D In_2Se_3 atop a metallic electrode, defined as $E_b = E_{M+2D} - E_{2D} - E_M$. Here, E_{2D} and E_M denote the energies of isolated monolayer In_2Se_3 and the electrode, respectively, while E_{M+2D} represents the total energy of the bilayer. We consider three phases of In_2Se_3: α, β', and β, all observed experimentally.[31−34] In the case of the α-In_2Se_3-based bilayer heterostructure, there are two configurations to consider. One has $\mathcal{P}_{OP}$ pointing away from the electrode, and the other has $\mathcal{P}_{OP}$ pointing toward the electrode, labeled as α_{up} and α_{dn} in Figure 2a, respectively.

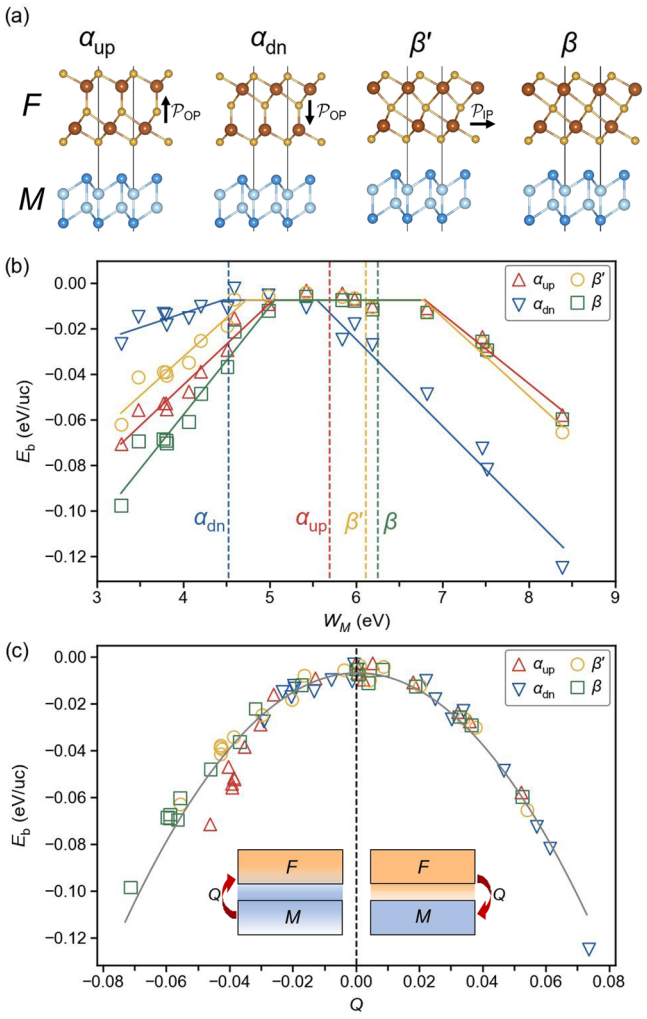

Figure 2. (a) Monolayer In_2Se_3 atop an electrode for binding energy (E_b) calculations. 2D metallic materials with lattice constants comparable with α-In_2Se_3 are chosen as the electrodes. The specific electrode shown here is Ti_2I_2 (W_M = 3.28 eV) with I and Ti atoms colored in dark blue and light blue, respectively. (b) Volcano-type relationships between E_b and electrode work function W_M for four different bilayer configurations. Vertical dashed lines mark the work functions of In_2Se_3 in different phases and polar states. (c) E_b as a function of the quantity of charge transfer (Q) at the interface. The gray line is the quadratic fit, $E_b = -\gamma Q^2$.

As illustrated in Figure 2b, the plots of E_b versus W_M curves reveal volcano-type relationships with flattened tops for all bilayer heterostructures. For a specific configuration of In_2Se_3, the magnitude of E_b decreases (becomes less negative) nearly linearly with the increasing W_M value within the LW region. This is followed by a W_M-insensitive zone (flattened top) when W_M is comparable to the work function of In_2Se_3 (W_{2D}, represented by vertical dashed lines in Figure 2b). In the HW region where W_M is substantially greater than W_{2D}, the binding strength increases with increasing W_M. Importantly, when the In_2Se_3 layer is electron-doped by the adjacent LW electrode (W_M < 4.5 eV), the nonpolar β phase exhibits the strongest interaction with the electrode, followed by α_{up} and β', with α_{dn} being the weakest. This sequence largely aligns with the order of W_{2D}: β has the highest at 6.3 eV, followed by α_{up} at 5.6 eV and α_{dn} at 4.5 eV. We note that the work functions of α_{up} and α_{dn} correspond to the work functions of negatively charged and positively charged surfaces of α-In_2Se_3, respectively, and their difference arises from the built-in depolarization field across the monolayer.[35,36] In contrast, in the HW region (W_M > 6.5 eV), α_{dn} with the lowest work function interacts most strongly with the electrode, whereas the other three types of In_2Se_3 monolayers have comparable binding energies. These volcano-type relationships cannot be explained by the screening effect. Instead, the evident dependence of E_b on the difference between W_M and W_{2D} highlights the importance of the interfacial charge transfer.

We find that the distinct volcano-type relationships presented in Figure 2b can be consolidated into a single scaling relationship between E_b and the amount of charge (Q) transferred at the interface. A negative Q indicates electron transfer from the electrode to monolayer In_2Se_3, typically occurring in the LW region. The hole doping (Q > 0) of the monolayer In_2Se_3 is observed near the HW electrodes. Remarkably, as shown in Figure 2c, the binding energies of 72 bilayer heterostructures (constructed using 18 electrodes and 4 states of 2D In_2Se_3) are well captured by the quadratic equation $E_b = -\gamma Q^2$, with γ = −19.7 V/e. This quadratic scaling of E_b with Q naturally explains the volcano-type relationships between E_b and W_M, as $|Q|$ is proportional to $|W_{2D} - W_M|$. The W_M-insensitive plateaus correspond to weak-charge-transfer regions, where $|Q|$ < 0.05 e/uc. Results from these model calculations demonstrate conclusively that charge transfer dictates the binding strength between the electrode and the monolayer. The observed universal quadratic relationship, $E_b = -\gamma Q^2$, can be understood by using a parallel plate capacitor model. The interaction energy between two oppositely charged plates, separated by a distance d and carrying charges $\pm Q$, is given by $E = -\frac{Q^2}{8\pi\epsilon_0 d}$, where ϵ_0 is the vacuum permittivity. This naturally leads to a quadratic dependence on Q, providing an intuitive explanation for $E_b \propto -Q^2$.

The pronounced interaction between monolayer β-In_2Se_3 and LW electrodes implies that the β phase might become energetically favored over the α phase in an MFM trilayer when E_b overcompensates for the intrinsic energy difference between these two phases. This is confirmed by DFT calculations on realistic capacitor models with atomic positions fully relaxed, while vdW correction is also implemented during structural optimizations. Two trilayer heterostructures are considered, labeled as MαM and MβM (see the insets in Figure 3a). Their relative thermodynamic stability is gauged by the energy difference defined as $\Delta E = E(M\alpha M) - E(M\beta M)$. It is easy to derive that

$$\Delta E \propto [E^{OC}(\alpha) - E^{OC}(\beta)] + [E_b(\alpha_{up}) + E_b(\alpha_{dn}) - 2E_b(\beta)] \quad (1)$$

https://doi.org/10.1021/acs.nanolett.4c01362
Nano Lett. XXXX, XXX, XXX−XXX

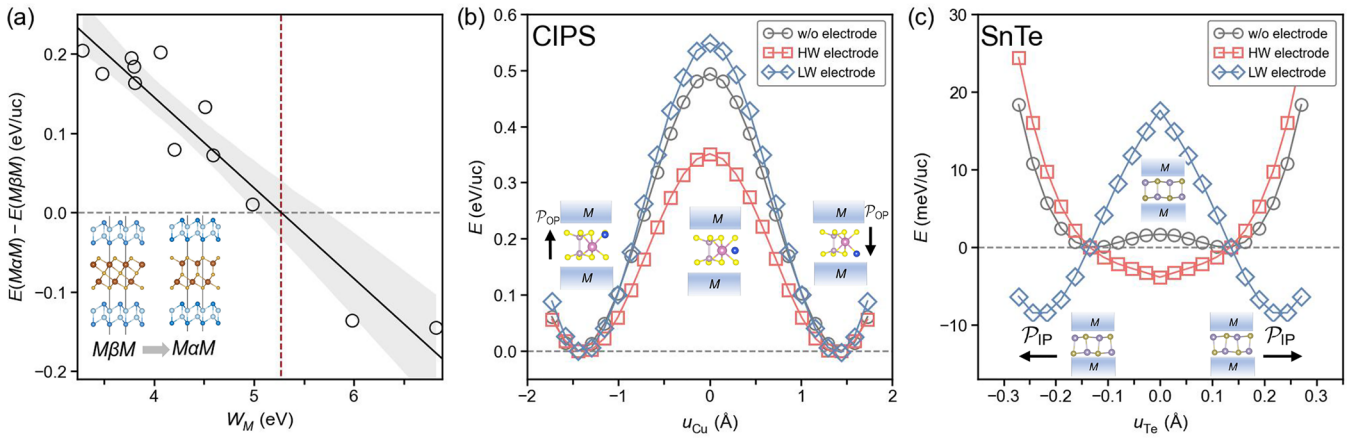

Figure 3. (a) Relative thermodynamic stability between MαM and MβM as a function of W_M. The solid black line represents the linear fit, and the gray area represents the 95% confidence region. The vertical red dashed line marks the critical value of W_M, below which the MβM capacitor configuration is more stable than MαM. Switching barriers in monolayer (b) $CuInP_2S_6$ and (c) SnTe without and with electrodes.

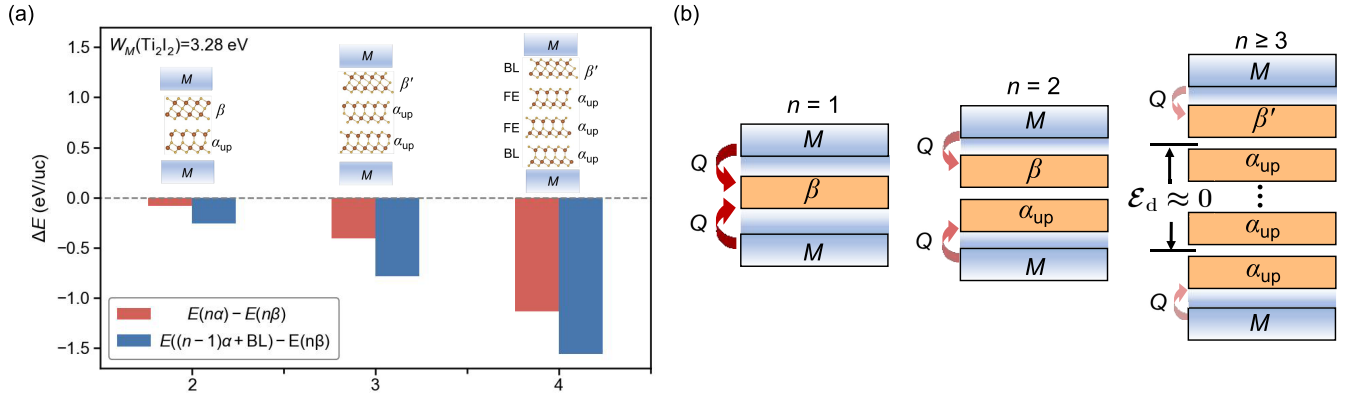

Figure 4. (a) Evolution of relative stability of n layers of In_2Se_3 sandwiched between Ti_2I_2 electrodes. The energy of an MFM consisting of n layers β-In_2Se_3, denoted as $n\beta$, is chosen as the energy reference. The capacitor with $n - 1$ layers of α-In_2Se_3 and one buffer layer (BL) has the lowest energy. The BL adopts the β phase at $n = 2$ but the β' phase for $n \geq 3$. (b) Schematic illustrating the evolution of the capacitor's structure with increasing thickness of the ferroelectric layer due to the competing charge transfer and screening effects.

Since the freestanding monolayer α-In_2Se_3 is more stable than β-In_2Se_3, $E^{OC}(\alpha) - E^{OC}(\beta) < 0$. However, if $E_b(\beta)$ is significantly more negative than $E_b(\alpha_{up})$ and $E_b(\alpha_{dn})$, the second (positive) term in eq 1 overcompensates for the first negative term, reversing the thermodynamic stability between the α and β phases. Indeed, as Figure 3a illustrates, MβM is more stable ($\Delta E > 0$) than MαM for electrodes with $W_M < 5.3$ eV, whereas MαM becomes the favorable configuration for HW electrodes.

The significant influence of interfacial charge transfer on ferroelectric stability is a common characteristic of 2D ferroelectric-based capacitors. Taking CIPS with $\mathcal{P}_{OP}$ and SnTe with $\mathcal{P}_{IP}$ as examples, we calculate the switching barriers under SC electrical boundary conditions (ΔU^{SC}) with electrodes of LW and HW, respectively (see computational details in the Supporting Information). As shown in Figure 3b, the presence of HW electrodes substantially lowers the switching barrier in monolayer CIPS by 0.14 eV/uc. This effect can be understood as follows. Analogous to eq 1, the magnitude of ΔU^{SC} can be approximated by the energy difference between the ferroelectric (FE) phase and the reference paraelectric (PE) phase in a capacitor

$$\Delta U^{SC} \propto \Delta U^{OC} + [2E_b(\mathrm{PE}) - E_b(\mathrm{FE_{up}}) - E_b(\mathrm{FE_{dn}})] \quad (2)$$

where $\Delta U^{OC} \approx E^{OC}(\mathrm{PE}) - E^{OC}(\mathrm{FE})$ is the switching barrier in an isolated monolayer. Contrary to β-In_2Se_3, the paraelectric phase of CIPS exhibits a stronger binding affinity to HW electrodes than does its ferroelectric phase, with E_b(PE) being more negative than E_b(FE). As a result, HW electrodes enhance the stability of the paraelectric phase relative to the ferroelectric phase, effectively lowering the switching barrier (red line). Moreover, the ferroelectric phases of CIPS demonstrate stronger interaction strengths with LW electrodes than the paraelectric phase, resulting in ΔU^{SC} being higher than ΔU^{OC} (blue line). For monolayer SnTe encapsulated by HW electrodes, the effect of charge transfer is similar to that in CIPS: the paraelectric phase is stabilized by HW electrodes more than the ferroelectric phase. Since ΔU^{OC} (1.3 meV) is small in SnTe,[24] the in-plane ferroelectricity is then fully suppressed, leading to a nonpolar ground state. Interestingly, LW electrodes promote in-plane ferroelectricity, indicated by an increased switching barrier and a ground state characterized by larger ferroelectric displacements (Figure 3c). These findings indicate that despite the distinct E_b–W_M relationships in different 2D ferroelectrics, the significant role of interfacial charge transfer in influencing the ferroelectric stability within

https://doi.org/10.1021/acs.nanolett.4c01362
Nano Lett. XXXX, XXX, XXX−XXX

an MFM capacitor is a common characteristic across these materials.

A pertinent question naturally arises: how does the increasing thickness of the ferroelectric layer influence its stability, particularly considering the competing effects of charge transfer and screening from the electrodes? Since HW electrodes already stabilize α-In_2Se_3 at the monolayer limit, our discussion below will focus on LW electrodes, represented by Ti_2I_2 (W_M = 3.28 eV). We fully optimized the atomic positions of an MFM capacitor consisting of n layers of In_2Se_3 sandwiched between Ti_2I_2 electrodes. In the case of n = 2, the bilayer α-In_2Se_3 becomes more stable than the bilayer β-In_2Se_3, as reported in Figure 4a. According to eq 1, it is straightforward to derive $\Delta E = E(\mathrm{M}n\alpha\mathrm{M}) - E(\mathrm{M}n\beta\mathrm{M}) = n[E^{\mathrm{OC}}(\alpha) - E^{\mathrm{OC}}(\beta)] + [E_b(\alpha_{up}) + E_b(\alpha_{dn}) - 2E_b(\beta)]$. As the first term, negative and representing bulk contribution, scales with n and the interfacial contribution remains nearly constant, it is unsurprising that the intrinsic thermodynamic stability of the α phase dominates. Interestingly, in the lowest-energy configuration, the bottom layer is in the polar α phase, while the top layer adopts the nonpolar β phase functioning as a buffer layer (BL; see the insets in Figure 4a). This suggests that $|E^{\mathrm{OC}}(\alpha) - E^{\mathrm{OC}}(\beta)| < E_b(\alpha_{dn}) - E_b(\beta)$. For $n \geq 3$, the capacitor with a BL, denoted as $(n-1)\alpha$ + BL, is always energetically favored over the multilayer α-In_2Se_3, denoted as $n\alpha$. An intriguing difference from the n = 2 case is that BL adopts the β' phase instead of the β phase. Detailed charge analysis reveals that the amount of charge transferred from the top electrode to the adjacent β-In_2Se_3 decreases with increasing thickness (see the Supporting Information). Since E_b scales with Q^2, the reduced binding affinity at n = 3 is insufficient to stabilize β-In_2Se_3 over β'-In_2Se_3. The evolution of the capacitor's structure with increasing thickness of the ferroelectric layer is illustrated in Figure 4b. The spontaneous formation of an asymmetric capacitor with symmetric electrodes could be important for the design of ferroelectric tunneling junctions.

In summary, we have investigated the interplay between the interfacial charge transfer and screening effects in 2D ferroelectric capacitors. The key difference between these two effects is that the screening effect dose does not depend on the work function of the electrode, while charge transfer strongly depends on the work function difference between the ferroelectric and the adjacent metal electrode. Consequently, the screening effect plays an important role in thicker capacitors due to its Coulombic nature, whereas charge transfer strongly affects the layer adjacent to the electrode, making it primarily a local effect. Our extensive model calculations of 72 bilayer heterostructures, involving monolayer In_2Se_3 in different phases and polar states sandwiched by 2D metallic electrodes, reveal a volcano-type relationship between the binding energy and electrode work function. Distinct volcano-type relationships observed among various phases and polar states of In_2Se_3 can be unified into a robust quadratic correlation linking the binding energy with the amount of charge transferred at the interface. At the monolayer limit, it is the interfacial charge transfer that determines the relative thermodynamic stability among competing In_2Se_3 phases in an MFM capacitor. This significant role of interfacial charge transfer in dictating ferroelectric stability and switching barriers is also observed in $CuInP_2S_6$ and SnTe, confirming its prevalent importance across 2D ferroelectrics. With increased ferroelectric layer thickness, we observe a transition from a charge-transfer-dominant regime to a screening-dominant regime. In capacitors with multilayer In_2Se_3, the spontaneous emergence of a buffer layer next to the electrode on one side leads to an inherently asymmetric structure. The insights gained from this study provide useful guidelines for the future design and optimization of next-generation ferroelectric nanoelectronic devices, underlining the significance of interface engineering in these applications.

■ ASSOCIATED CONTENT

Supporting Information

The Supporting Information is available free of charge at https://pubs.acs.org/doi/10.1021/acs.nanolett.4c01362.

Details about 2D metallic electrodes; charge doping effect on monolayer In_2Se_3; ferroelectric asymmetric capacitors; switching barriers of $CuInP_2S_6$ and SnTe; charge analysis of 2D ferroelectric capacitors (PDF)

■ AUTHOR INFORMATION

Corresponding Author

Shi Liu − *Key Laboratory for Quantum Materials of Zhejiang Province, Department of Physics, School of Science, Westlake University, Hangzhou, Zhejiang 310030, China;* orcid.org/0000-0002-8488-4848; Email: liushi@westlake.edu.cn

Authors

Jiawei Huang − *Key Laboratory for Quantum Materials of Zhejiang Province, Department of Physics, School of Science, Westlake University, Hangzhou, Zhejiang 310030, China;* orcid.org/0000-0002-4387-6294

Changming Ke − *Key Laboratory for Quantum Materials of Zhejiang Province, Department of Physics, School of Science, Westlake University, Hangzhou, Zhejiang 310030, China;* orcid.org/0000-0002-2018-2441

Zhuang Qian − *Key Laboratory for Quantum Materials of Zhejiang Province, Department of Physics, School of Science, Westlake University, Hangzhou, Zhejiang 310030, China*

Complete contact information is available at: https://pubs.acs.org/10.1021/acs.nanolett.4c01362

Author Contributions

#J.H. and C.K. contributed equally.

Notes

The authors declare no competing financial interest.

■ ACKNOWLEDGMENTS

We acknowledge the support from the National Natural Science Foundation of China (52002335) and the Westlake Education Foundation. The computational resources are provided by the Westlake HPC Center.

■ REFERENCES

(1) Ding, W.; Zhu, J.; Wang, Z.; Gao, Y.; Xiao, D.; Gu, Y.; Zhang, Z.; Zhu, W. Prediction of intrinsic two-dimensional ferroelectrics in In_2Se_3 and other III_2-VI_3 van der waals materials. *Nat. Commun.* **2017**, *8*, 14956.

(2) Xiao, J.; Zhu, H.; Wang, Y.; Feng, W.; Hu, Y.; Dasgupta, A.; Han, Y.; Wang, Y.; Muller, D. A.; Martin, L. W.; Hu, P.; Zhang, X. Intrinsic two-dimensional ferroelectricity with dipole locking. *Phys. Rev. Lett.* **2018**, *120*, 227601.

(3) Liu, F.; You, L.; Seyler, K. L.; Li, X.; Yu, P.; Lin, J.; Wang, X.; Zhou, J.; Wang, H.; He, H.; Pantelides, S. T.; Zhou, W.; Sharma, P.; Xu, X.; Ajayan, P. M.; Wang, J.; Liu, Z. Room-temperature

ferroelectricity in $CuInP_2S_6$ ultrathin flakes. *Nat. Commun.* **2016**, *7*, 12357.
(4) Brehm, J. A.; Neumayer, S. M.; Tao, L.; O'Hara, A.; Chyasnavichus, M.; Susner, M. A.; McGuire, M. A.; Kalinin, S. V.; Jesse, S.; Ganesh, P.; Pantelides, S. T.; Maksymovych, P.; Balke, N. Tunable quadruple-well ferroelectric van der Waals crystals. *Nat. Mater.* **2020**, *19*, 43.
(5) Zheng, Z.; Ma, Q.; Bi, Z.; de la Barrera, S.; Liu, M.-H.; Mao, N.; Zhang, Y.; Kiper, N.; Watanabe, K.; Taniguchi, T.; Kong, J.; Tisdale, W. A.; Ashoori, R.; Gedik, N.; Fu, L.; Xu, S.-Y.; Jarillo-Herrero, P. Unconventional ferroelectricity in moiré heterostructures. *Nature* **2020**, *588*, 71.
(6) Stern, M. V.; Waschitz, Y.; Cao, W.; Nevo, I.; Watanabe, K.; Taniguchi, T.; Sela, E.; Urbakh, M.; Hod, O.; Shalom, M. B. Interfacial ferroelectricity by van der Waals sliding. *Science* **2021**, *372*, 1462.
(7) Rogée, L.; Wang, L.; Zhang, Y.; Cai, S.; Wang, P.; Chhowalla, M.; Ji, W.; Lau, S. P. Ferroelectricity in untwisted heterobilayers of transition metal dichalcogenides. *Science* **2022**, *376*, 973.
(8) Wu, M.; Li, J. Sliding ferroelectricity in 2d van der waals materials: Related physics and future opportunities. *Proc. Natl. Acad. Sci. U. S. A.* **2021**, *118*, No. e2115703118.
(9) Miao, L.-P.; Ding, N.; Wang, N.; Shi, C.; Ye, H.-Y.; Li, L.; Yao, Y.-F.; Dong, S.; Zhang, Y. Direct observation of geometric and sliding ferroelectricity in an amphidynamic crystal. *Nat. Mater.* **2022**, *21*, 1158.
(10) Ielmini, D.; Wong, H.-S. P. In-memory computing with resistive switching devices. *Nat. Electron.* **2018**, *1*, 333.
(11) Yu, H.; Chung, C.-C.; Shewmon, N.; Ho, S.; Carpenter, J. H.; Larrabee, R.; Sun, T.; Jones, J. L.; Ade, H.; O'Connor, B. T.; So, F. Flexible inorganic ferroelectric thin films for nonvolatile memory devices. *Adv. Funct. Mater.* **2017**, *27*, 1700461.
(12) Si, M.; Saha, A. K.; Gao, S.; Qiu, G.; Qin, J.; Duan, Y.; Jian, J.; Niu, C.; Wang, H.; Wu, W.; Gupta, S. K.; Ye, P. D. A ferroelectric semiconductor field-effect transistor. *Nat. Electron* **2019**, *2*, 580.
(13) Zhang, Y.; Wang, L.; Chen, H.; Ma, T.; Lu, X.; Loh, K. P. Analog and digital mode α-In_2Se_3 memristive devices for neuromorphic and memory applications. *Adv. Electron. Mater.* **2021**, *7*, 2100609.
(14) Wan, S.; Li, Y.; Li, W.; Mao, X.; Wang, C.; Chen, C.; Dong, J.; Nie, A.; Xiang, J.; Liu, Z.; Zhu, W.; Zeng, H. Nonvolatile ferroelectric memory effect in ultrathin α-In_2Se_3. *Adv. Funct. Mater.* **2019**, *29*, 1808606.
(15) Garcia, V.; Bibes, M. Ferroelectric tunnel junctions for information storage and processing. *Nat. Commun.* **2014**, *5*, 4289.
(16) Junquera, J.; Ghosez, P. Critical thickness for ferroelectricity in perovskite ultrathin films. *Nature* **2003**, *422*, 506.
(17) Xue, F.; He, X.; Ma, Y.; Zheng, D.; Zhang, C.; Li, L.-J.; He, J.-H.; Yu, B.; Zhang, X. Unraveling the origin of ferroelectric resistance switching through the interfacial engineering of layered ferroelectric-metal junctions. *Nat. Commun.* **2021**, *12*, 7291.
(18) Gerra, G.; Tagantsev, A. K.; Setter, N.; Parlinski, K. Ionic polarizability of conductive metal oxides and critical thickness for ferroelectricity in $BaTiO_3$. *Phys. Rev. Lett.* **2006**, *96*, 107603.
(19) Yang, J.; Zhou, J.; Lu, J.; Luo, Z.; Yang, J.; Shen, L. Giant tunnelling electroresistance through 2D sliding ferroelectric materials. *Mater. Horiz.* **2022**, *9*, 1422−1430.
(20) Wang, Y.; Liu, X.; Burton, J. D.; Jaswal, S. S.; Tsymbal, E. Y. Ferroelectric instability under screened coulomb interactions. *Phys. Rev. Lett.* **2012**, *109*, 247601.
(21) Zhang, S.; Zhu, Y.; Tang, Y.; Liu, Y.; Li, S.; Han, M.; Ma, J.; Wu, B.; Chen, Z.; Saremi, S.; Ma, X. Giant polarization sustainability in ultrathin ferroelectric films stabilized by charge transfer. *Adv. Mater.* **2017**, *29*, 1703543.
(22) Lin, Y.; Shao, Y.; Dai, J.; Li, T.; Liu, Y.; Dai, X.; Xiao, X.; Deng, Y.; Gruverman, A.; Zeng, X. C.; Huang, J. Metallic surface doping of metal halide perovskites. *Nat. Commun.* **2021**, *12*, 7.
(23) Wu, J.; Bai, L.; Huang, J.; Ma, L.; Liu, J.; Liu, S. Accurate force field of two-dimensional ferroelectrics from deep learning. *Phys. Rev. B* **2021**, *104*, 174107.
(24) Liu, K.; Lu, J.; Picozzi, S.; Bellaiche, L.; Xiang, H. Intrinsic origin of enhancement of ferroelectricity in SnTe ultrathin films. *Phys. Rev. Lett.* **2018**, *121*, 027601.
(25) Kresse, G.; Furthmuller, J. Efficient iterative schemes for *ab initio* total-energy calculations using a plane-wave basis set. *Phys. Rev. B* **1996**, *54*, 11169.
(26) Kresse, G.; Furthmuller, J. Efficiency of ab-initio total energy calculations for metals and semiconductors using a plane-wave basis set. *Comput. Mater. Sci.* **1996**, *6*, 15.
(27) Perdew, J. P.; Burke, K.; Ernzerhof, M. Generalized gradient approximation made simple. *Phys. Rev. Lett.* **1996**, *77*, 3865.
(28) Blochl, P. E. Projector augmented-wave method. *Phys. Rev. B* **1994**, *50*, 17953.
(29) Haastrup, S.; Strange, M.; Pandey, M.; Deilmann, T.; Schmidt, P. S.; Hinsche, N. F.; Gjerding, M. N.; Torelli, D.; Larsen, P. M.; Riis-Jensen, A. C.; Gath, J.; Jacobsen, K. W.; Mortensen, J. J.; Olsen, T.; Thygesen, K. S. The computational 2D materials database: high-throughput modeling and discovery of atomically thin crystals. *2D Mater.* **2018**, *5*, 042002.
(30) Gjerding, M. N.; Taghizadeh, A.; Rasmussen, A.; Ali, S.; Bertoldo, F.; Deilmann, T.; Knøsgaard, N. R.; Kruse, M.; Larsen, A. H.; Manti, S.; Pedersen, T. G.; Petralanda, U.; Skovhus, T.; Svendsen, M. K.; Mortensen, J. J.; Olsen, T.; Thygesen, K. S. Recent progress of the computational 2D materials database (C2DB). *2D Mater.* **2021**, *8*, 044002.
(31) Chen, Z.; Sun, M.; Li, H.; Huang, B.; Loh, K. P. Oscillatory order−disorder transition during layer-by-layer growth of indium selenide. *Nano Lett.* **2023**, *23*, 1077.
(32) Zhang, F.; Wang, Z.; Dong, J.; Nie, A.; Xiang, J.; Zhu, W.; Liu, Z.; Tao, C. Atomic-scale observation of reversible thermally driven phase transformation in 2D In_2Se_3. *ACS Nano* **2019**, *13*, 8004.
(33) Zheng, X.; Han, W.; Yang, K.; Wong, L. W.; Tsang, C. S.; Lai, K. H.; Zheng, F.; Yang, T.; Lau, S. P.; Ly, T. H.; Yang, M.; Zhao, J. Phase and polarization modulation in two-dimensional In_2Se_3 via in situ transmission electron microscopy. *Sci. Adv.* **2022**, *8*, No. eabo0773.
(34) Zheng, C.; Yu, L.; Zhu, L.; Collins, J. L.; Kim, D.; Lou, Y.; Xu, C.; Li, M.; Wei, Z.; Zhang, Y.; Edmonds, M. T.; Li, S.; Seidel, J.; Zhu, Y.; Liu, J. Z.; Tang, W.-X.; Fuhrer, M. S. Room temperature in-plane ferroelectricity in van der Waals In_2Se_3. *Sci. Adv.* **2018**, *4*, No. eaar7720.
(35) Huang, J.; Duan, X.; Jeon, S.; Kim, Y.; Zhou, J.; Li, J.; Liu, S. On-demand quantum spin hall insulators controlled by two-dimensional ferroelectricity. *Mater. Horiz.* **2022**, *9*, 1440.
(36) Ke, C.; Huang, J.; Liu, S. Two-dimensional ferroelectric metal for electrocatalysis. *Mater. Horiz.* **2021**, *8*, 3387.

https://doi.org/10.1021/acs.nanolett.4c01362
Nano Lett. XXXX, XXX, XXX−XXX